MADRID
inter.noise 2019
June 16 - 19
NOISE CONTROL FOR A BETTER ENVIRONMENT

L_1 regularisation in the inverse method for the synthesis of indoor tyre pass-by noise

Papaioannou, Athanasios[1], Elliott, Stephen[2], Cheer, Jordan[3]
University of Southampton
University Road, SO17 1BJ, Southampton, UK

ABSTRACT

The indoor pass-by noise measurement can nowadays be realised in a laboratory environment with a stationary vehicle on a rolling road and a microphone array, according to ISO – 362-1:2016. Within this indoor testing procedure, there is also the option of evaluating the different contributions from the various noise sources on a car, for example using the inverse method with a number of sensors close to the various sources. This work assumes a 2D-tyre model to approximate the behaviour of a real car tyre at low frequencies. The inverse method is then adopted using this model for the tyre noise contribution synthesis and corresponding source strength and synthesised pressure estimates are calculated. A novel regularisation method is finally investigated to further optimise the far field pass-by noise pressure estimates.

Keywords: Pass-By, Tyre noise, Inverse method
I-INCE Classification of Subject Number: 11

1. INTRODUCTION

The exterior sound emission of a vehicle is an increasingly important criterion for the homologation of road vehicles. Until recently, pass-by noise has been measured outdoors, but can now be measured in an indoor environment with a stationary vehicle on a rolling bench and a microphone array, according to ISO-362-1:2016 [1]. In-room pass-by noise testing systems using a roller bench in a semi-anechoic room offers numerous advantages for engineering purposes. The total repeatability of the measurements is very high, while the capability to distinguish between the various car noise source contributions enables engineers to gain more insight into the root causes of the overall noise disturbance.

Pass-by noise contribution analysis is typically realised by using a number of additional microphones in close proximity to the real car sources. Each source is approximated by a set of uncorrelated point sources and an inverse method is then implemented in order to quantify the various noise source distributions [2-6].

[1] ap3m17@soton.ac.uk
[2] s.j.elliott@soton.ac.uk
[3] j.cheer@soton.ac.uk

To accomplish this inverse identification procedure, acoustic transfer responses are measured between all point sources and all microphone positions to allow full matrix coupling between all sources and indicators, while the synthesis of the acoustic pressure in the far field is realised by using a linear sensor array at 7.5 m away from the car. An alternative to the traditional methods is that presented by Janssens et al who further simplified the inverse problem by omitting the phase information in an energetic, power-based inverse approach [7].

Within the work described above, the equivalent point source positions have been predefined based on the physical insight of the car source noise generating mechanisms. With the aim of overcoming this limitation, the work presented herein utilises corresponding regularisation methods that can effectively optimise the positions of the chosen equivalent point sources for the tyre pass-by noise contribution synthesis.

2. THE TYRE MODEL

The tyre noise contribution is approximated herein by using a 2D linear tyre model, following the work done by Rustighi and Elliott in [8].

2.1 The ring model

The tyre model used here is the stationary ring model, as described in [8] and originally proposed by Huang and Soedel [9]. In this model, the stiffness of the sidewalls, the inflation pressure and the loss factors of sidewalls, tread and internal pressure have been taken into account. However, the model only includes the vibration of the belt, not the sidewalls and it does not take into account the effects due to the rotation and the anti-symmetric rigid belt modes, since these can only be represented by a 3D model. Therefore, it can be used to account for the dominant tyre response below about 400 Hz, above which the first cross modes and aerodynamic sources become apparent. The tyre tread and sidewall are assumed to be divided up into N_T discrete elements. By substituting a trial solution for the distributed forces, the natural frequencies and the mode shapes of the system are found. Hence, the vector of complex radial velocities at the centre of each element, $\boldsymbol{v_T}$, are related to the vector of complex forces acting on the elements, $\boldsymbol{f_T}$, via the matrix of structural mobilities for the free tyre suspended off the ground, $\boldsymbol{Y_T}$, so that

$$\mathbf{v_T} = \mathbf{Y_T f_T} \, . \tag{1}$$

The two-dimensional ring can provide a good approximation to the behaviour of a real car tyre in the low-frequency range given that the parameters of the model are properly tuned to the tyre characteristics. In Figure 1, the experimental setup of a car tyre measured in the SPCG Lab at the University of Southampton is shown.

Figure 1. Experimental setup of the car tyre measurement

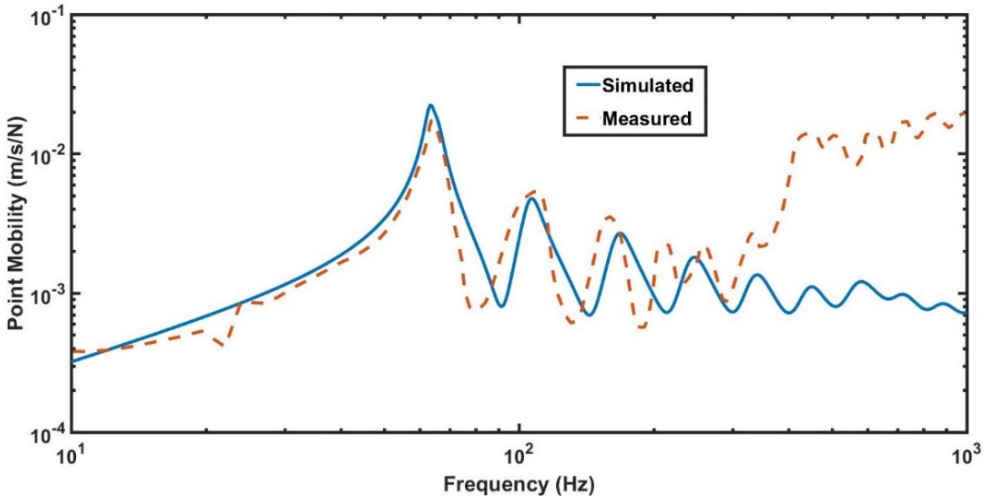

Figure 2. Simulated and measured point mobility response (10 Hz – 1 kHz)

In Figure 2, the measured point radial mobility is shown over frequency, along with the one calculated using the model described above. These results show that the measurements are in very good agreement with the simulated results from 10 Hz up to approximately 300 Hz, while there is a deviation between the results above 300 Hz. In the stiffness controlled region (10 – 70 Hz), the mobility is slightly underestimated in the measured results, while there is also a spike present in all various mobility graphs between 20 – 25 Hz due to a resonance of the support structure. From 70 to 300 Hz, the circumferential modes are more closely spaced in the measurements, possibly due to the difficulty in accurately modelling the elastic properties of the tyre. Above 300 Hz, the model tends to underestimate the mobility of the tyre as the high frequency tendency towards plate-like behavior seen in the measurements is not included in the model.

2.2 The contact model

A very simplified contact model is used here in which it is assumed that all of the contact patch is in contact with the road at all times and that only a set of isolated, locally acting springs generate the contact stiffness, which is called a Winkler bedding. In this case, the spectral density matrix for the contact forces can be calculated from a statistical model of the road roughness using a linear analysis.

The tyre is assumed to be in contact with the road using such a linear contact model, which gives rise to the vector of driving forces, $\boldsymbol{f_T}$. Such a model consists of a Winkler bedding of N_C independent springs that connect each point on the road with vertical displacement d to each point in the contact patch on the tyre with vertical tyre displacement w. The force at all N_T points on the tyre is related to the difference between the road and tyre displacements by the linear equation

$$\mathbf{f_T} = \mathbf{K_{TC}}(\mathbf{d} - \mathbf{w}) \tag{2}$$

where $\boldsymbol{d}$ and $\boldsymbol{w}$ are $N_C \cdot 1$ vectors of the vertical displacement of the road and tyre in the contact patch and $\boldsymbol{K_{TC}}$ is an $N_T \cdot N_C$ matrix describing the linear contact stiffness.

The vector of radial velocities for the tyre due to the road roughness can then be calculated as

$$\mathbf{v_T} = \mathbf{T}\mathbf{d} \tag{3}$$

where the overall transfer matrix, $\boldsymbol{T}$, is equal to $\boldsymbol{Y_F[I + K_{TC}C_{CT}]^{-1}K_{TC}}$ and $\boldsymbol{C_{CT}}$ is the $N_C \cdot N_T$ matrix of tyre compliances at the points in the contact patch.

2.3 The road excitation

The excitation of the tyre running over a rough road is modelled as a random displacement distribution with a specified spatial correlation. For a vehicle travelling at a constant velocity, the displacement can be considered as a realisation of a multi-variate stationary random process and so can be described by a spectral density matrix. Each contact point travels over the same profile as that of the forward contact points, so that each point experiences, after a speed-dependent delay, the same imposed displacement. The individual complex displacements are grouped in an $N_C \cdot 1$ vector, $\boldsymbol{d}$, and the spectral density matrix is then given by

$$\mathbf{S_{dd}} = \mathrm{E}[\mathbf{d}\mathbf{d}^{\mathbf{H}}] \tag{4}$$

where E is the expectation operator and ^{H} the Hermitian, transpose. The time varying road displacement $d(t)$ is derived from traversing, at vehicle velocity v, a rigid road profile, as shown in [8].

2.4 Tyre – road interaction results

The combination of the tyre, contact and tyre excitation models leads to a fully linear model in which random vibration analysis theory can be applied. The spectral density matrix of the tyre's radial velocities, $\boldsymbol{S_{vv}}$, due to the road excitation can be expressed in terms of the road displacement spectral density matrix, $\boldsymbol{S_{dd}}$, as

$$\mathbf{S_{vv}} = \mathbf{T}\mathbf{S_{dd}}\mathbf{T}^{\mathbf{H}} . \tag{5}$$

Therefore, it is possible to express in one equation the relationship between road profile and tyre vibration. The radial velocity distribution around the tyre can then be calculated from the diagonal elements of $\boldsymbol{S_{vv}}$. In Figure 3, the rms element velocity is given for various car velocities by integrating the velocity distribution over a frequency range of 10 Hz – 1 kHz.

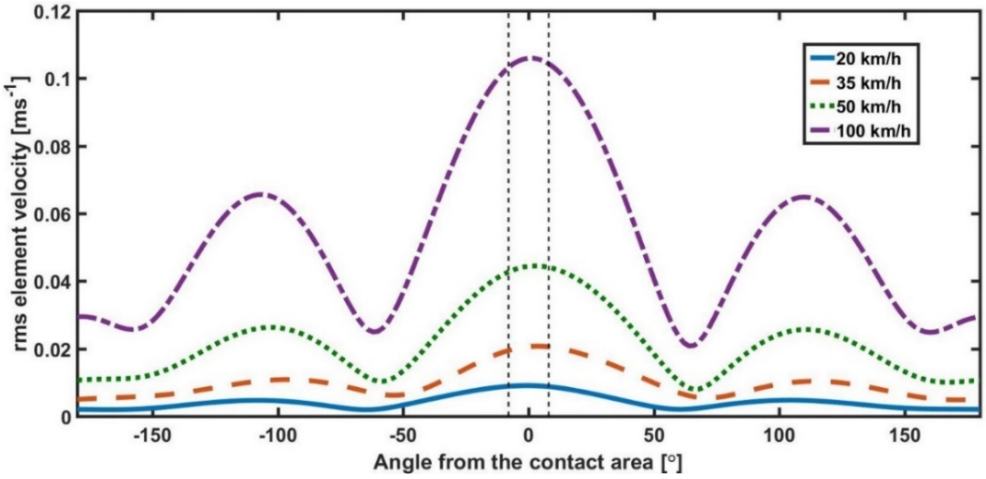

Figure 3. Root mean square of the tyre element radial velocity, evaluated at different car speeds. The dashed vertical lines denote the extent of the contact patch.

As expected, the tyre velocity at the contact patch is much larger than in the rest of the tyre, and it falls off away from the contact patch, because of the high damping of the rubber material. This radial velocity distribution is used herein to approximate the tyre noise contribution within an indoor pass-by noise testing procedure.

3. APPLICATION OF INVERSE METHOD TO TYRE PASS-BY NOISE SYNTHESIS

In this section, the formulation of the inverse method for the tyre pass-by noise contribution synthesis is given, as described in [10] for a line source.

3.1 Use of near field source estimates for far field pressure reconstruction

The model considers the tyre as a circular source of length L = 0.56 m equal to its diameter. A polar microphone array, consisting of 32 sensors, is used covering 300^0 along an arc of radius 0.65L, excluding a region of 60^0 close to the contact patch, as shown in Figure 4(a). A linear microphone array at 7.5 m away from the tyre is also used, as shown in Figure 4(b).

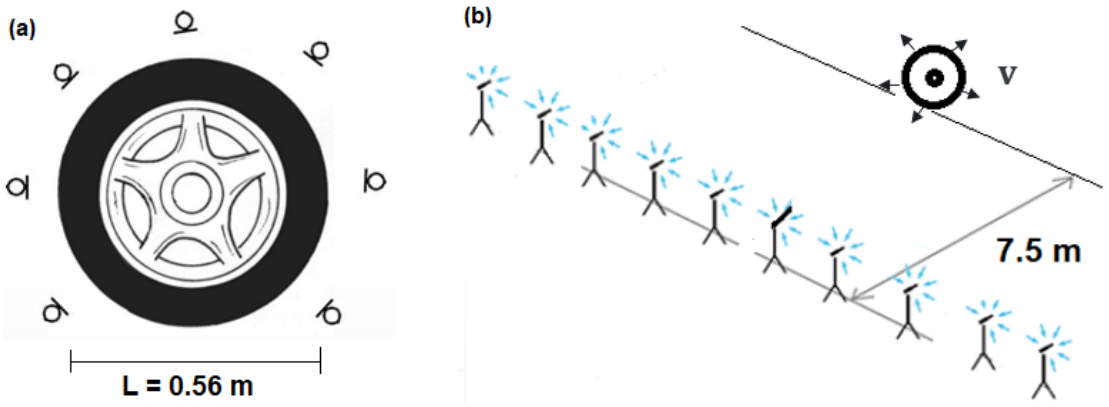

Figure 4.(a) Schematic of the tyre and the polar microphone array in the near field, (b) Schematic of the tyre and the linear microphone array in the far field

The radiation from the tyre is approximated by using the spectral density matrix of the radial tyre velocities. The matrix of pressure cross spectra at the microphones is then given by [10]

$$\mathbf{S_{pp,near}} = \mathbf{G S_{vv} G^H} \tag{6}$$

where $\boldsymbol{S_{vv}}$ is the radial tyre velocity spectral density matrix and $\boldsymbol{G}$ is the matrix of (3D free-space) Green functions, linking each radial source velocity to each pressure, such that

$$G_{m,n} = \frac{j\rho_o \omega e^{-j\omega r_{m,n}/c_0}}{4\pi r_{m,n}} \tag{7}$$

where $r_{m,n}$ is the distance from tyre element n to microphone m and c_0 is the speed of sound. To this end, the tyre source is divided into a small number of equivalent sources and the inverse method is applied to the pressure cross spectra defined in Equation 6 using the inverse (or, more generally, the pseudo-inverse $\boldsymbol{G}^+$) of the matrix of Green functions $\boldsymbol{G}$. This yields an estimate of a simplified source cross-spectral matrix, such that [10]

$$\hat{\mathbf{S}}_{\mathbf{vv}} = \mathbf{G^+ S_{pp} G^{+H}}\,. \tag{8}$$

This estimate is then used to calculate the far field power spectra for a linear microphone array at 7.5 m away from the tyre, as shown in Figure 4(b). An estimate of the pressures at the sensors using the simplified source distribution is then given by

$$\hat{\mathbf{S}}_{\mathbf{pp,far}} = \mathbf{G}\hat{\mathbf{S}}_{\mathbf{vv}}\mathbf{G^H} \tag{9}$$

which can be compared to the exact directly radiated field $\boldsymbol{S_{pp,far}}$ to give a root mean square error in dB between the exact and reconstructed pressure fields averaged over all M microphones, as given by

$$E = \frac{1}{M}\sum_{m=1}^{M}\left|10\log_{10}\left\{\left|\frac{\hat{p}_{m,m}}{p_{m,m}}\right|\right\}\right| \quad \text{(dB)} \qquad (10)$$

where $p_{m,m}$ is the mth diagonal component of S_{pp} etc., and M is the number of microphones.

3.2 Results

The equivalent sources are uniformly positioned covering the whole tyre circumference, when 4, 8 or 16 equivalent sources are assumed. When the source number is smaller (2 sources), they are placed very close to the tread pattern. For values of kL = 2.57, 6.7, 10.2 (f = 200 Hz, 650 Hz and 1 kHz respectively), the near field 4 - element reconstructed source distributions and the corresponding magnitude of their reconstructed pressure directivities in the far field are given in Figure 5.

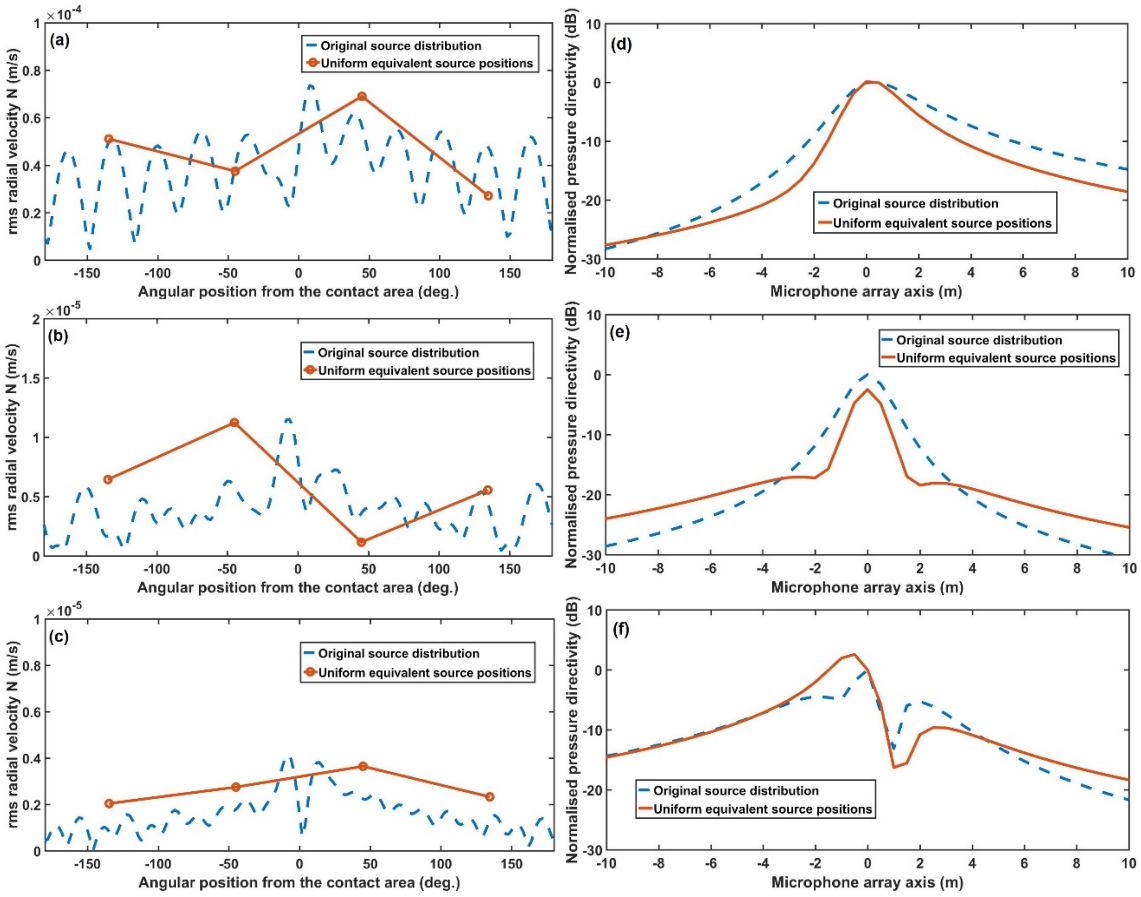

Figure 5(a),(b),(c). Comparison between original and near field reconstructed source distribution: 4 equivalent sources, kL = 2.57, 6.7 and 10.2, (d),(e),(f) Comparison between direct and synthesized far field pressure directivity, kL = 2.57, 6.7 and 10.2

In Figures 5(a), (b) and (c), the original source distribution is compared with the uniformly spaced equivalent one. The inverse method does not reproduce the short wavelength components of the radial velocity, but focuses on the long wavelength components. In Figures 5(d), (e) and (f), it is also shown that despite the errors in the

reconstructed source distribution, the synthesised far field directivity is a good representation of the direct field because the short-wavelength components in the reconstructed source distributions, which are not reproduced with only a few equivalent sources, do not radiate efficiently into the far field. However, as frequency increases, the errors in the reconstructed source distribution do not increase significantly, but errors in the radiated pressure far field have become more apparent.

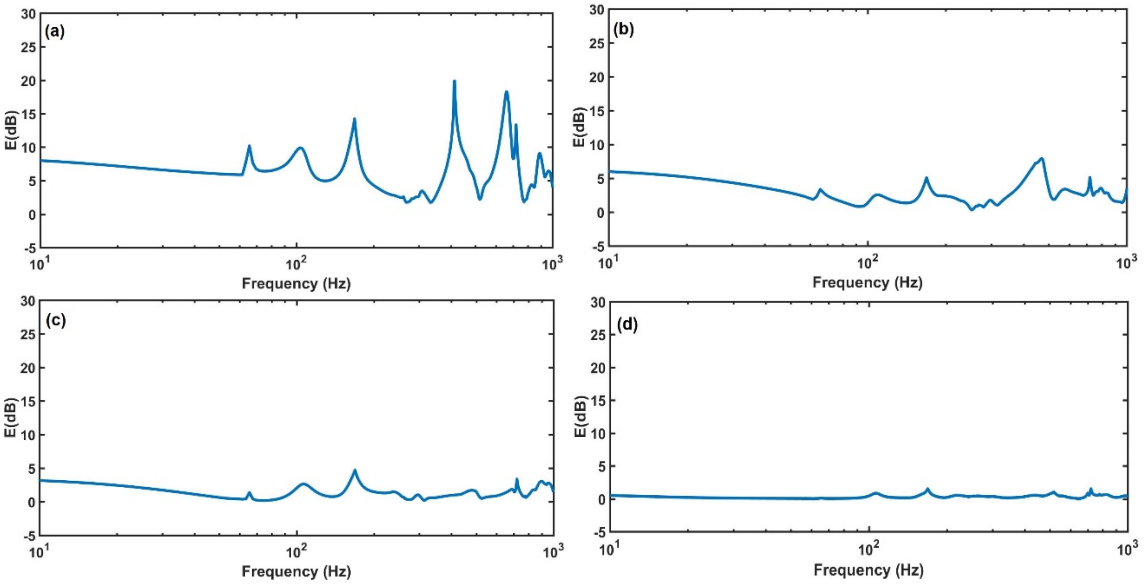

Figure 6. dB error in near field reconstructed far field sound pressure for various number of source elements: (a) 2 source elements, (b) 4 source elements, (c) 8 source elements and (d) 16 source elements

Figures 6(a)-(d) show the error E in the reconstructed pressure far field, as in Equation 10, as a function of frequency using a simplified source distribution of 2, 4, 8 and 16 elements respectively. As noted above, in the 2-element case the source positions have been chosen to be very close to the tread pattern, while for a larger number of elements (4 and above) the source positions have been chosen uniformly spaced across the circumference of the tyre. It is shown that as the number of equivalent source elements increases, the error decreases correspondingly towards 0 dB which would indicate no error. The high error levels are due to the use of the ill-conditioned inverse method, associated with the conditioning of the Green function matrices. At lower frequencies, the condition number rises rapidly when the number of equivalent sources is too small and the accuracy of the inversion is subsequently limited. At higher frequencies, the conditioning of the transfer matrices improves and the errors are mostly associated with the number of equivalent sources per wavelength required for the spatial sampling criterion to be satisfied.

In practice, there are two methods that may be used to improve the accuracy of the inverse problem. The first involves regularisation of the Green function matrices to reduce the number of possible degrees of freedom in the problem [11-12] and the second one, selecting the optimum number and spacing of source elements for each frequency. This work focuses on the second one and introduces an l_1 – norm penalty in the inverse problem which effectively optimises the equivalent source positioning within the source reconstruction process.

4. USE OF L_1 – NORM REGULARISATION

As stated above, the simplified equivalent source positions used in Section 3 have been predefined for a given number of elements. In general, the conditioning is strongly dependent on the geometry of the problem, which means that it can be controlled, to a large extent, by careful choice of the number and spacing of source elements as a function of frequency. Therefore, this means that the accuracy of the inversion can be improved by optimising the equivalent source geometry.

In this section, the optimisation of the source number and position is realised by using the sparsity – promoting properties of the l_1-norm regularisation technique, widely known as the Lasso method. This is a Compressive Sensing method (CS) and is designed to identify both correlated and uncorrelated distributed sources up to frequencies where the average array inter-element spacing is significantly larger than half of the wavelength [13].

4.1 Formulation

Within the method, the power spectral matrix of the pressure distribution $\boldsymbol{S}_{pp,near}$ is analysed with an eigenvalue factorisation [14]

$$\mathbf{S}_{pp,near} = \mathbf{V}\mathbf{S}\mathbf{V}^{\mathrm{H}} \tag{11}$$

where $\mathbf{V}$ is a unitary matrix with the columns containing the eigenvectors $\mathbf{v}_\mu$, $\mu = 1, 2, ..., M$ and $\mathbf{S}$ is a diagonal matrix with the real non-negative eigenvalues on the diagonal. Each eigenvector represents a coherent signal across the microphones under the constraint of orthogonality. Based on the factorisation in Equation (11), the Principal Components of the pressure $\mathbf{p}_\mu$ can be calculated as

$$\mathbf{p}_{\boldsymbol{\mu}} = \mathbf{V}^{\mathbf{H}}\mathbf{p} \ . \tag{12}$$

These principal components represent the eigenmodes of the sound field, that is the eigenvector including its magnitude. The selection method is applied independently to each one of them and, subsequently, the output is added on a power basis since they represent incoherent parts of the sound field. In this paper, the selection method is used by only taking into account the first eigenmode for the frequency range of interest since this is found to give accurate results. The problem can therefore be described in linear matrix – vector notation as

$$\mathbf{p_1} = \mathbf{G}\mathbf{v_1} \tag{13}$$

where $\boldsymbol{G}$ is the Green function matrix, $\mathbf{p_1}$ is the principal component derived by the first eigenmode and $\mathbf{v_1}$ is the corresponding radial velocity component. The configuration used in this problem is more flexible, meaning that the circumference of the tyre is filled with 40 equally spaced virtual point sources. The minimised cost function is then given by

$$\min\|\mathbf{p_1} - \mathbf{G}\mathbf{v_1}\|_2^2 \text{ subject to} \|\mathbf{v_1}\|_1^1 \leq \delta \ . \tag{14}$$

This convex optimisation problem is solved by using the SPGL1 toolbox [15]. The computational demand for the problem is high because no analytic solution exists. However, the utilisation of this Lasso technique gives the opportunity to choose the number of sources with which the source reconstruction is realised from a total number of 40 candidate sources. The l1 norm of the source velocity distribution promotes sparsity which is adjusted by tuning the regularisation parameter δ. The smaller the regularisation parameter δ is chosen, the more it is going to enforce sparsity in the solution and thus a

smaller number of non-zero equivalent sources, but that will happen at the cost of a loss of reconstruction accuracy. The level of the regularisation parameter δ essentially provides a trade off between accuracy and the number of equivalent sources involved in the inversion.

4.2 Results

For values of kL = 2.57, 6.7, 10.2 (f = 200 Hz, 650 Hz and 1 kHz respectively), the parameter δ was adjusted until there were only 4 dominant equivalent sources. The near field reconstructed source distributions, selected as described above, and the corresponding magnitude of their reconstructed pressure directivities in the far field are given in Figure 7.

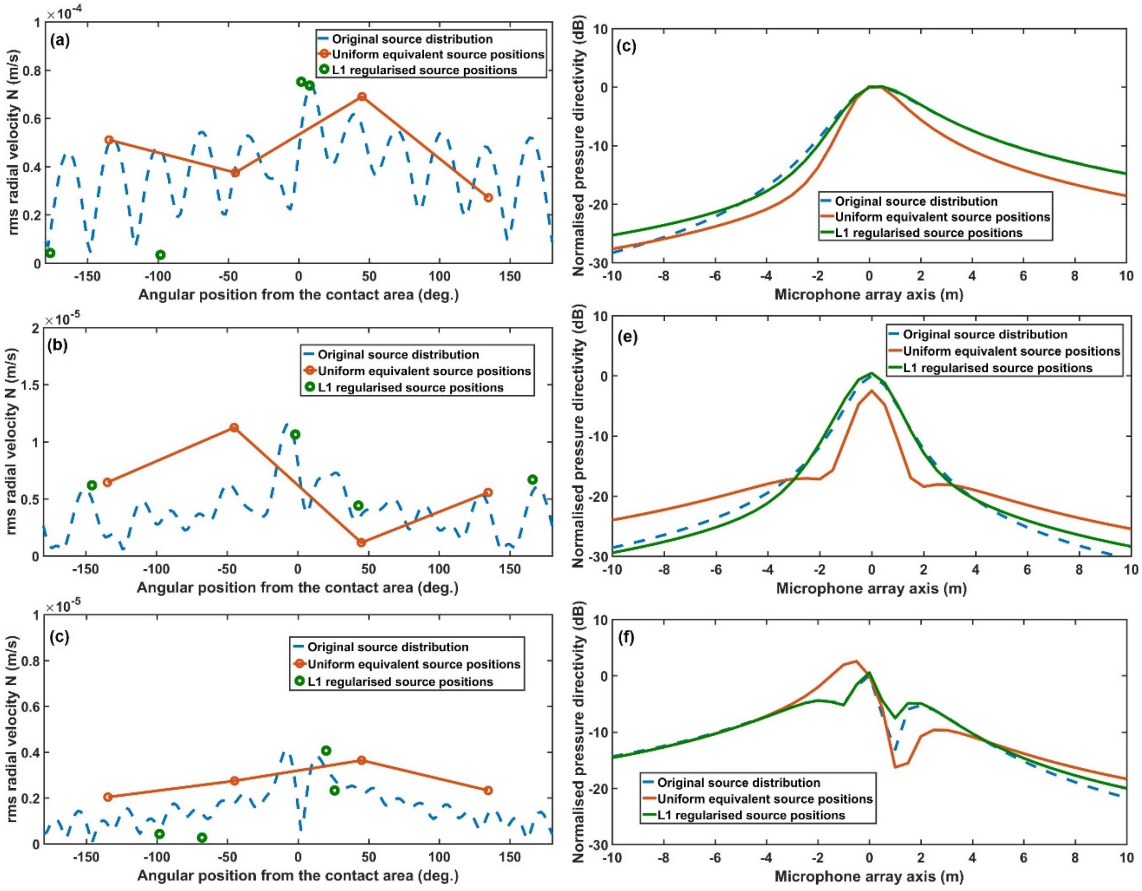

Figure 7(a),(b),(c). Comparison between original and near field reconstructed source distribution: 4 equivalent sources either chosen to give uniform spacings(orange) as in Section 3 or chosen to give the best least squares solution (green) as in Section 4, kL = 2.57, 6.7 and 10.2, (d),(e),(f) Comparison between direct and synthesized far field pressure directivities, kL = 2.57, 6.7 and 10.2

It is clear from Figure 7(a), (b) and (c) that the l1-norm minimization chooses a different equivalent source distribution of four elements with irregular spacing compared to the uniform one. This results in an improved far field pressure directivity at the three frequencies examined here, as shownn in Figure 7(d), (e) and (f). It is also shown that at 200 Hz the point sources tend to group together in larger size sources as the pressure directivity results are similar if δ is adjusted to give only 3 equivalent sources. In the 650 Hz and 1 kHz cases, the point sources tend to spread out a bit more across the tyre circumference, forming smaller size sources. This phenomenon is better illustrated if the

sparsity criterion is relaxed and the number of point sources is increased. At lower frequencies, a small number of block sources is then created, while at higher frequencies a larger distribution of small sources is formed. This observation is in accordance with the spatial sampling criterion which requires a large number of small elements to minimise spatial aliasing at high frequencies and a smaller number of large elements at lower frequencies.

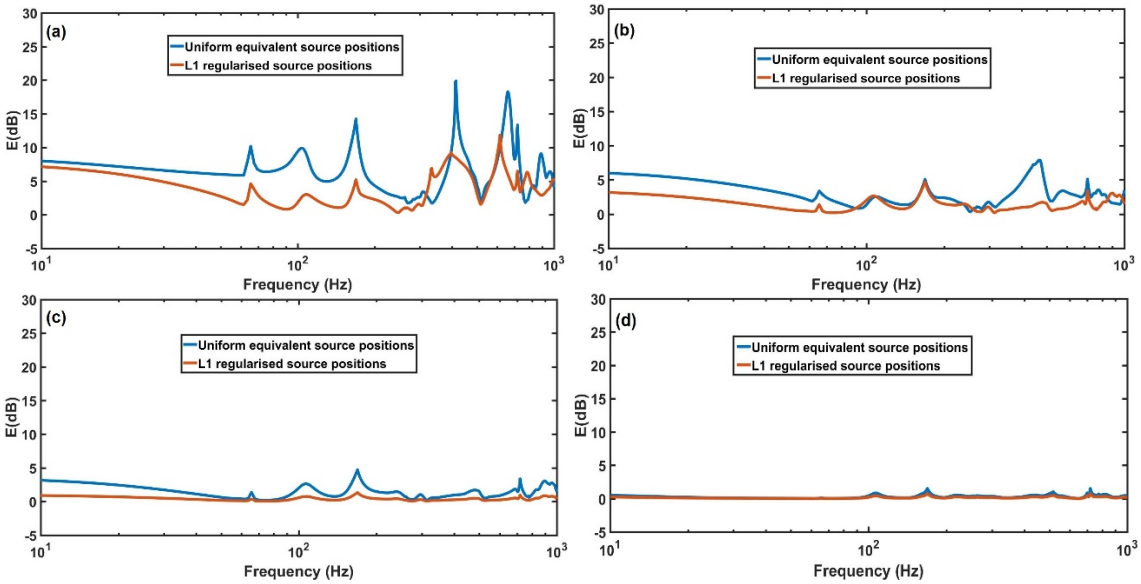

Figure 8. dB error in near field reconstructed far field pressures for various number of source elements: (a) 2 source elements, (b) 4 source elements, (c) 8 source elements and (d) 16 source elements chosen with the methods described in Sections 3 and 4

Fig. 8(a)-(d) shows the error *E* in the reconstructed pressure field as a function of frequency using a simplified source distribution of 2, 4, 8 and 16 elements respectively. From these results it can be seen that optimising the positions of the equivalent sources improves the source reconstruction when using the near field array and, thus improves the far field directivity estimates in the frequency range of interest. The effect of the method is mostly visible when using a small number of sources as the errors decrease significantly, especially at lower frequencies.

5. CONCLUSIONS

In this paper, an application of the inverse method to the indoor synthesis of tyre pass-by noise contribution is studied. The tyre noise contribution is represented by a 2D-tyre model, which does not take into account the acoustic sources but can be a very good approximation to the vibration of a real car tyre, especially at lower frequencies. The tyre model is then embedded into a model of the acoustic radiation where the far field pressure directivity is synthesised by using a polar array in close proximity to the tyre and then compared to the one radiated directly in the far field linear array. Within this method, the equivalent source positions on the tyre circumference are predefined. In the last section, an additional l1-norm regularisation term is embedded in the inverse method, which optimises the positioning of the equivalent sources by choosing from a number of candidate sources on the tyre circumference. The final optimised far field pressure directivities are compared to the direct and the near-field synthesised ones and it is shown that very small synthesis errors can be achieved in the frequency range of interest with careful selection of the regularisation parameter.

6. ACKNOWLEDGEMENTS

The authors gratefully acknowledge the European Commission for its support of the Marie Sklodowska Curie program through the ETN PBNv2 project (GA 721615).

7. REFERENCES

1. International Organization for Standardization, **ISO 362-3:2016**: Measurement of noise emitted by accelerating road vehicles -- Engineering method -- Part 1: M and N categories, pp. 51

2. A. Schuhmacher, Y. Shirahashi, M. Hirayama, Y. Ryu, Indoor pass-by noise contribution analysis using source path contribution concept, *Proceedings of the 2012 International Conference on Modal Analysis Noise and Vibration Engineering (ISMA)*, Leuven (2012), pp. 3697-3709.

3. F. Bianciardi, K. Janssens, M. Choukri, H. Van Der Auweraer, 'Indoor pass-by noise engineering: a motorbike application case', *Proceedings of Inter-Noise 2014*, Melbourne (2014)

4. D. Arsic, 'Efficient testing by combining simulated pass-by measurements and OTPA', Muller-BBM VibroAkustik Systeme, Technical Paper

5. U. Kim, M. Maunder, P. Grant, D. Mawdsley, 'Developing a Car to Meet New Pass-By Noise Requirements using Simulation and Testing', *SAE Technical Paper* 2015-01-2319, 2015

6. Z. Chu, H. Wang, C. Chen, H. Yan, R. Kang, 'Source Path Contribution Analysis for Vehicle Indoor Pass-By Noise', *SAE Technical Paper* 2017-01-2247, 2017

7. K. Janssens, P. Aarnoutse, P. Gajdatsy, L. Britte, F. Deblauwe, H. Van der Auwerauer, 'Time-Domain Source Contribution Analysis Method for In-Room Pass-by Noise', *SAE Technical Paper* 2011-01-1609, 2011

8. E. Rustighi, S.J. Elliott, Stochastic road excitation and control feasibility in a 2D linear tyre model, *Journal of Sound and Vibration* 300 (2007) 490-501.

9. S. Huang, W. Soedel, Effects of coriolis acceleration on the free and forced in-plane vibrations of rotating rings on elastic foundation, *Journal of Sound and Vibration* 115 (2) (1987) 253–274.

10. K.R. Holland, P.A. Nelson, The application of inverse methods to spatially-distributed acoustic sources, *Journal of Sound and Vibration* 332 (2013) 5727-5747.

11. P.A. Nelson, S.H. Yoon, Estimation of acoustic source strength by inverse methods: Part 1, conditioning of the inverse problem, *Journal of Sound and Vibration* 233 (4) (2000) 643-668.

12. S.H. Yoon , P.A. Nelson, Estimation of acoustic source strength by inverse methods: Part II, experimental investigation of methods for choosing regularization parameters, *Journal of Sound and Vibration* 233 (4) (2000) 669-705.

13. G. Chandon, L. Daudet, A. Peillot, F. Olivier, N. Bertin, R. Gribonval, 'Near-field acoustic holography using sparse regularisation and compressive sampling principles', *Journal of the Acoustic Society of America* 132 (3), pp. 1521-1534, 2012

14. J. Hald,'Fast wideband acoustical holography', *Journal of the Acoustical Society of America*, 139 (4), pp. 1508-1057, 2016

15. E. van den Berg and M. P. Friedlander, 'SPGL1: A solver for large-scale sparse reconstruction,' http://www.cs.ubc.ca/labs/scl/spgl1